

Electronic Supplementary Information

NiFe Layered double hydroxide-Decorated N-Doped Entangled-Graphene Framework: A Robust Water Oxidation Electrocatalyst

Narugopal Manna,^{a, b} Nadeema Ayasha,^{a, b} Santosh k. Singh,^c Sreekumar Kurungot,^{* a, b}

^aPhysical and Materials Chemistry Division, CSIR-National Chemical Laboratory, Pune-411008, India.

Email: k.sreekumar@ncl.res.in

^bAcademy of Scientific and Innovative Research (AcSIR), New Delhi-110001, India.

^cFaculty of Pure and Applied Sciences, University of Tsukuba, 1-1-1 Tennodai, Tsukuba, Ibaraki 305-8573, Japan.

Table and Contents

1.Experimental	S3
1.1. Materials.....	S3
1.2. Synthesis of Graphene oxide (GO).....	S3
2. Structural Characterization	S4
3. Electrochemical Studies	S5 & S6
4. Material and Electrochemical Characterizations	S6
Figure S1: TEM images of NiFe-LDH/EGF.....	S7
Figure S2: TEM images of unsupported NiFe-LDH.....	S7
Figure S3: EDS pattern of the NiFe-LDH/NEGF.....	S8
Figure S4: Comparative BET isotherms of NiFe-LDH/NEGF and NiFe-LDH/NEGF (w/o).....	S9
Figure S5: Comparative BET isotherms of NiFe-LDH/NEGF, and NiFe-LDH/NEGF(w/o).....	S9
Figure S6: Comparative BET isotherms of NEGF, NiFe-LDH, NiFe-LDH/NEGF, and NiFe-LDH/NEGF(w/o).....	S10
Figure S7: XPS analysis: (a) C 1s spectra of NEGF, (b) C 1s spectra of NEGF, (c) O 1s spectra of NiFe-LDH/NEGF, (d) O 1s spectra of NEGF and (e) N 1s spectra of NiFe-LDH/NEGF.....	S11
Figure S8: XPS analysis: (a) XPS spectra of Ni2p in NiFe-LDH and NiFe-LDH/NEGF. (b), XPS spectra of Fe2p in NiFe-LDH and NiFe-LDH/NEGF.....	S11
Figure S9: ECSA measurement through electrochemical double-layer charge capacitance (Cdl) measurement by recording CV in the non-Faradic region at different scan rates of 10 to 110 mV/s, (a) for NiFe-LDH, (b) for NiFe-LDH/NEGF(w/o), and (c) NiFe-LDH/NEGF...S12	
Figure S10: Comparative OER polarization curves of NiFe-LDH/NEGF and NiFe-LDH/EGF.....	S12
Figure S11: OER polarization curves recorded at 10 mV s ⁻¹ scan rate and 1600 rpm of the working electrode.....	S12

Figure S12: Nyquist plots recorded on rGO and NrGO at an applied potential of 1.57 V in the AC frequency range between 100 kHz and 0.1 Hz.....	S13
Table S1: EDS data table for NiFe-LDH/NEGF.	S8
Table S2. BET surface area values measured for the various catalysts.....	S10
Table S3: Comparison of the XPS data of the present work with the different works published in the literature.....	S11
Table S4: OER activity data Comparison for the different synthesized catalysts.....	S14
Table S5: Comparison of the OER activity data of the present work with the different works published in the literature.....	S14
5. References.....	S14

1. Experimental:

1.1. Materials.

Nickel acetate hexahydrate $[\text{Ni}(\text{OAc})_2 \cdot 6\text{H}_2\text{O}]$, iron acetate hexahydrate $[\text{Fe}(\text{OAc})_2 \cdot 6\text{H}_2\text{O}]$, ammonium hydroxide (NH_4OH), graphite and potassium permanganate (KMnO_4) were purchased from Sigma-Aldrich. Phosphoric acid (H_3PO_4) and sulphuric acid (H_2SO_4) were purchased from Thomas Baker. The entire chemical reagents were used as such without any further purification.

1.2. Synthesis of Graphene Oxide (GO):

Improved Hummer's method was employed for synthesizing graphene oxide (GO)¹. In brief, 3 g of graphite powder and 18 g of KMnO₄ were well mixed by using a mortar and pestle. After complete mixing, the powder was slowly added to the flask containing a solution mixture of H₃PO₄:H₂SO₄ (1:9) at 0 °C. After complete transfer of the solid combination, the temperature of the solution was increased slowly up to 60 °C and kept for 12 h at a constant temperature. After completion of the reaction, the solution mixture was held for a few hours with regular rotation to reach the temperature at room temperature. The obtained reaction mixture was slowly poured into ice-cooled water containing 3% H₂O₂, which lead to a yellowish solution. It was then washed several times with distilled water followed by centrifugation at 10000 rpm. The obtained solid residue was further washed with 30% HCl for the removal of any metal impurities. This was again washed with plenty of water to neutralize the acidic pH. Finally, a dark chocolate-colored highly viscous solution was obtained, which was further washed with ether and kept in an oven for drying at 40 °C.

2. Structural Characterization:

The morphological investigation and nanostructural distribution were performed using, field emission scanning electron microscopy (FESEM), and, transmission electron microscopy (TEM) respectively. FESEM analyses were carried out by FEI Nova Nano SEM 450 FESEM microscopes. TEM images were recorded on a Tecnai T-20 instrument at an accelerating voltage of 200 kV. The TEM sample was prepared by drop coating of the well-dispersed sample in isopropyl alcohol (1 mg of sample in 5 ml solvent) on a carbon coated 200 mesh copper grid. The sample-coated TEM grid was dried for 1 h under an IR-lamp. The as-synthesized sample's crystallinity was measured by the powder X-ray diffraction (PXRD) analysis. The XRD measurement was performed on a Rigaku Smart Lab diffractometer with Cu K α radiation ($\lambda = 1.5406 \text{ \AA}$) with a scan rate of 5° min^{-1} in the 2θ range of 5 to 80°. X-ray

photoelectron spectroscopy (XPS) was performed using a fully integrated, monochromated small spot X-ray photoelectron spectrometer (XPS) system. It is specified with the 180° double focussing hemispherical analyser-128-channel detector and micro-focused Al K α as X-ray monochromator source. Thermal stability of the material and the metal composite loading over the carbon were analysed using an SDT Q600 DSC-TDA thermo-gravimetric (TG) instrument in the temperature range of RT (Room Temperature)-900°C at a constant heating rate of 10 °C min⁻¹ in an oxygen atmosphere. Raman spectral investigations were carried out using 632 nm green laser (NRS 1500W) on an HR 800 RAMAN spectrometer. N₂ adsorption-desorption isotherm experiments were performed on a Quantachrome Quadrasorb automatic volumetric instrument to analyse the surface area and pore volume of the samples.

3. Electrochemical Studies:

The electrochemical data were acquired with the help of a set of electrochemical techniques including linear sweep voltammetry (LSV) using a rotating disc electrode (RDE) made of glassy carbon (0.0706 cm²) with the help of Pine Instrument. A three-electrode electrochemical cell was used with a SP-300 model BioLogic potentiostat. Hg/HgO was employed as the reference electrode, and graphite rod (Alfa Aesar, 99.99%) was used as a counter electrode. For OER performance comparison, we included the electrochemical activity of 20% RuO₂/C. RuO₂/C was prepared from commercial RuO₂ hydrate by adopting the procedure reported by Thomas Audichon *et al.*² The heat-treated RuO₂ was mixed with Vulcan carbon in the composition ratio of 1:4 to get 20% RuO₂/C. The catalyst slurry was prepared by mixing the catalyst (5 mg) in 1 mL isopropyl alcohol-water (3:2) solution and 40 μ L of Nafion solution (5 wt%, Sigma-Aldrich) using water-bath sonication for approximately 1 h. After well mixing, the catalysts slurry was coated on the surface of the working electrode, which was polished with 0.3 μ m alumina slurry in DI-water followed by cleaning with DI-water and acetone. 2.5 μ L of the ink was drop coated on the surface of the RDE

(0.0706 cm²) electrode. After coating the material on the electrode surface, the electrode was dried under an IR-lamp for 1 h. Catalyst coated dry electrode was prepared for the electrochemical study. An aqueous solution of 1 M KOH (de-aerated with nitrogen gas) was used as an electrolyte for the RDE experiments. All the electrode potentials were first converted into the reversible hydrogen electrode (RHE) through an RHE calibration experiment, which was done previously in our lab³, and for 1 M KOH, $E(\text{RHE}) = E(\text{Hg}/\text{HgO}) + 0.917 \text{ V}$. All the RDE experiments were carried out at a constant rotating rate of 1600 rpm in order to maintain a uniform ionic concentration of the reactant as well as to prevent accumulation of the products, *i.e.*, O₂ bubbles over the electrode surface. The linear sweep voltammetry data was corrected with 65% iR -compensation, where i and R indicate the current measured and the ohmic resistance employed between the working and reference electrode, respectively. Current densities were normalized by known value of electrode surface area and the reaction overpotential was determined using the equation: $\eta = [E(\text{RHE}) - 1.23] \text{ V}$. The Faradaic impedance was measured using the PEIS technique (Potentiostatic Electrochemical Impedance Spectroscopy) by using a SP-300 Biologic test station in the Faradaic region at 1.57 V *vs.* RHE covering the 100 KHz–0.1 Hz frequency range with 10 mV amplitude of sinusoidal potential perturbation as followed by J.F.C. Boodts *et al.*⁴ to study the Faradaic impedance of oxygen evolution reaction. All the impedance values are normalized with the electrode area of 0.0706 cm².

4. Material and Electrochemical Characterizations:

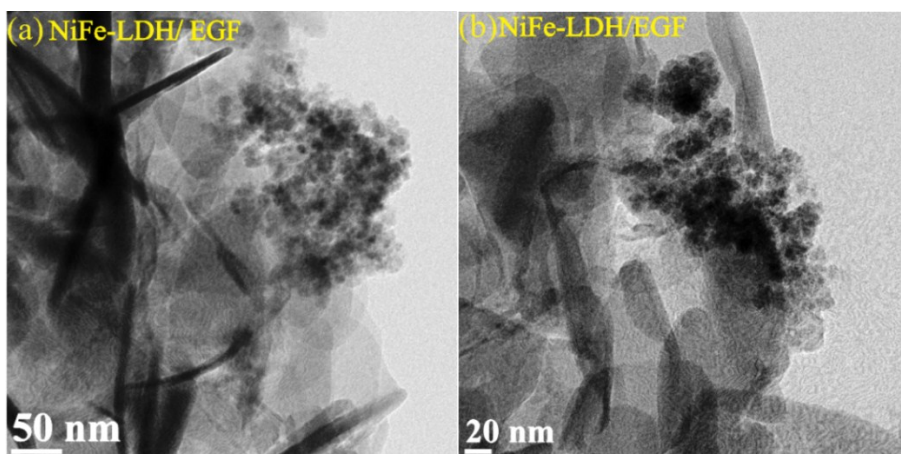


Figure S1: (a) and (b) are the TEM images of NiFe-LDH/EGF.

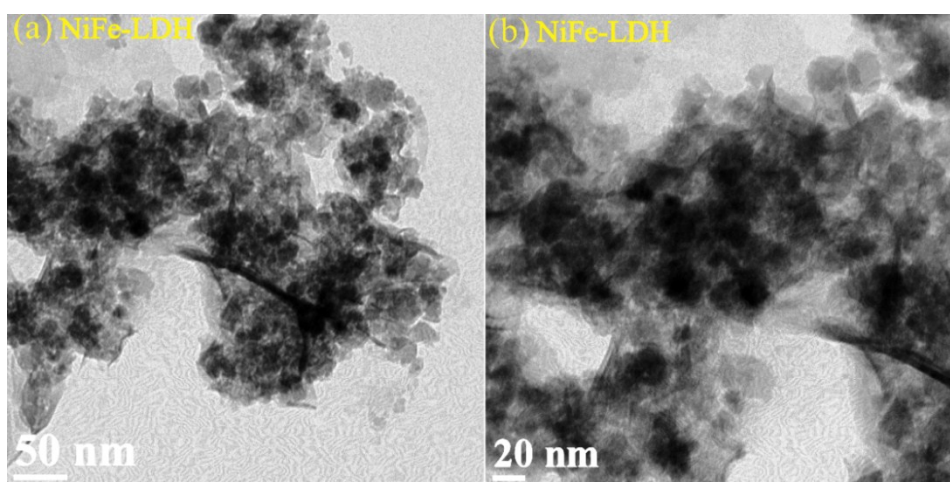


Figure S2: (a) and (b) are the TEM images of unsupported NiFe-LDH.



Figure S3: EDS pattern of the NiFe-LDH/NEGF

Table S1: EDS data table for NiFe-LDH/NEGF.

Element	Weight %	Atomic %
C K	52.13	64.08
N K	10.21	10.76
O K	23.25	21.45
Fe K	6.95	1.84
Ni K	7.46	1.88

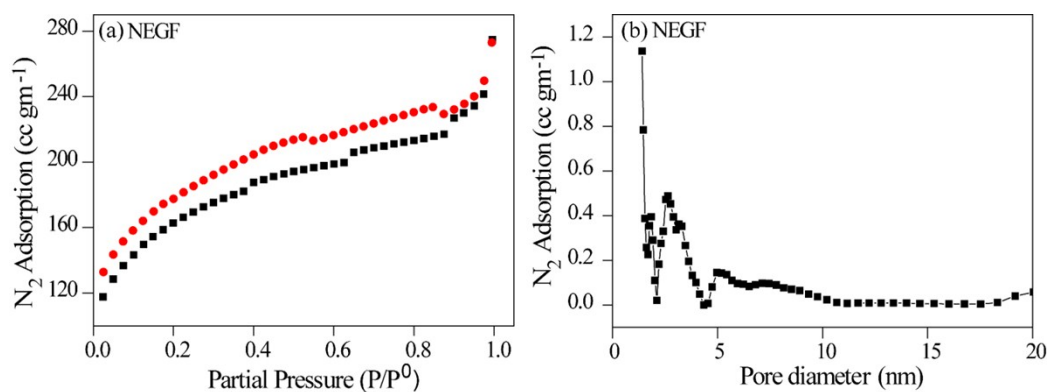


Figure S4: BET analysis of NEGF: a) adsorption-desorption isotherms and b) pore size distribution profile.

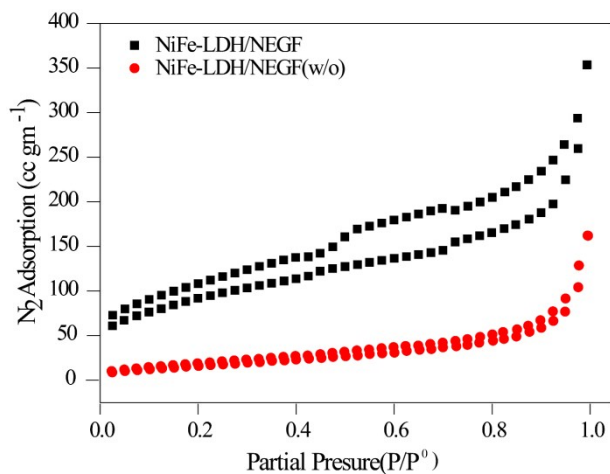


Figure S5: Comparative BET isotherms of NiFe-LDH/NEGF and NiFe-LDH/NEGF(w/o).

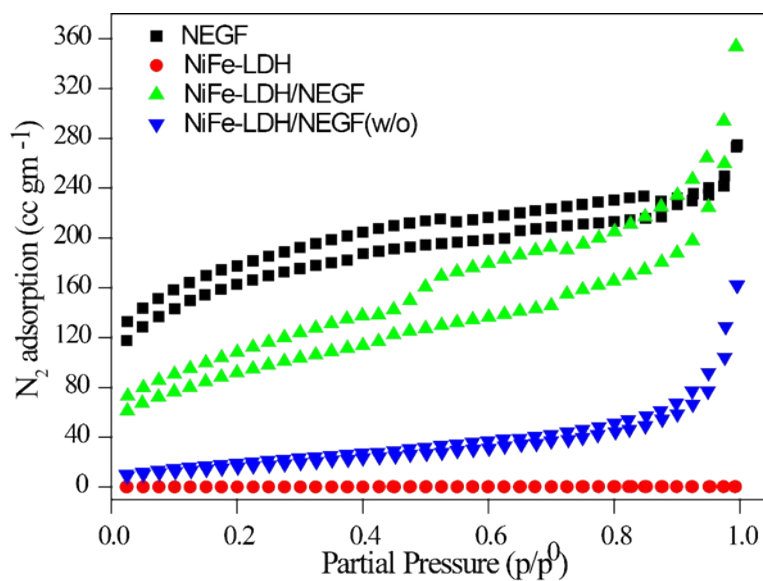


Figure S6: Comparative BET isotherms of NEGF, NiFe-LDH, NiFe-LDH/NEGF, and NiFe-LDH/NEGF(w/o).

Table S2. BET surface area values measured for the various catalysts.

<i>Catalyst</i>	<i>BET Surface Area (m²/g)</i>
<i>NiFe-LDH</i>	47.6
<i>GO</i>	298.0
<i>NEGF</i>	461.1
<i>NiFe-LDH/NEGF</i>	281.4

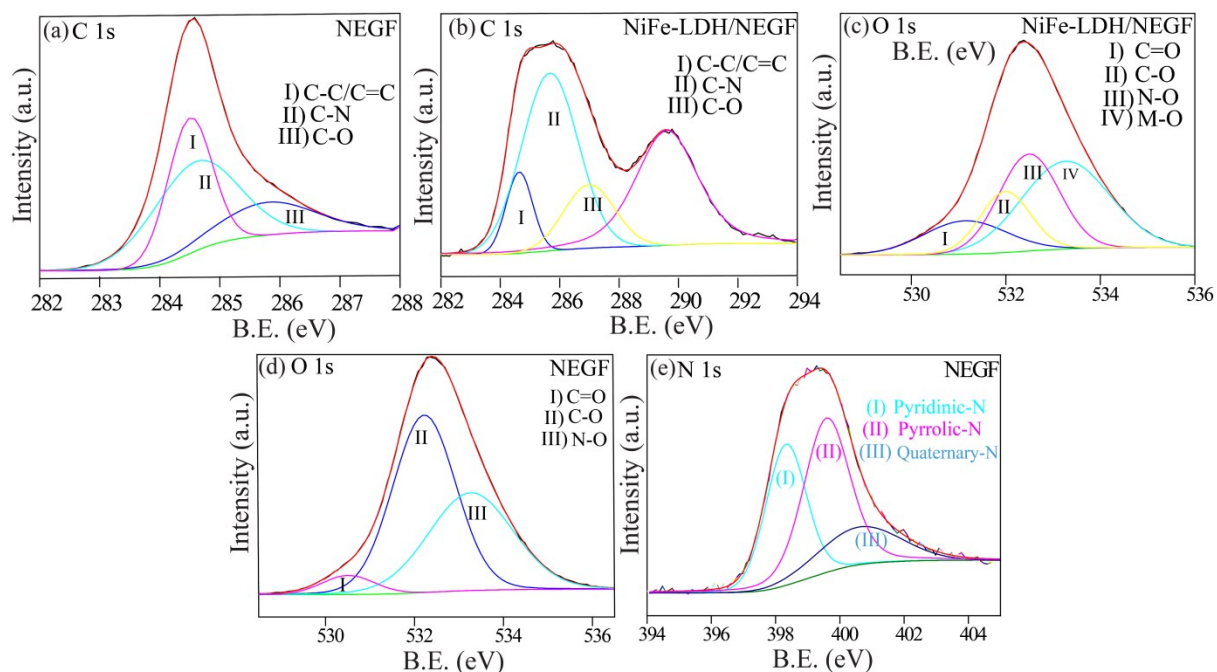


Figure S7: XPS analysis: (a) C 1s spectra of NEGF, (b) C 1s spectra of NiFe-LDH/NEGF, (c) O 1s spectra of NiFe-LDH/NEGF and (e) N 1s spectra of NiFe-LDH/NEGF.

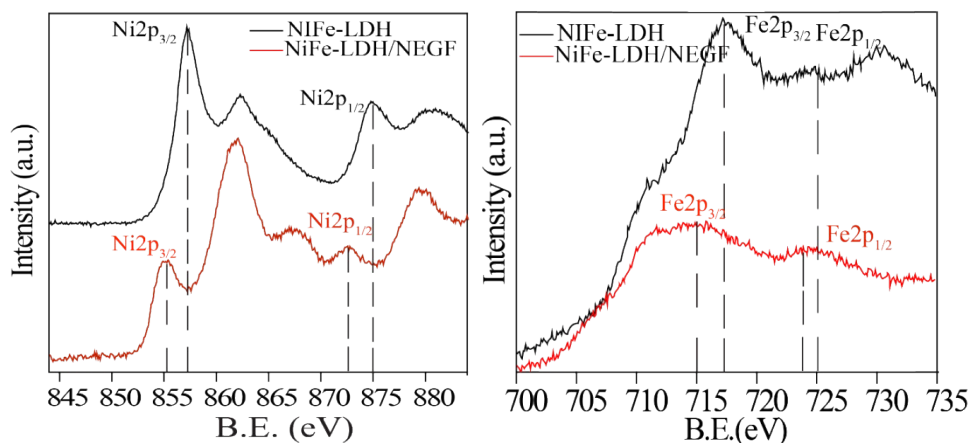


Figure S8: XPS analysis: (a) XPS spectra of Ni2p in NiFe-LDH and NiFe-LDH/NEGF. (b), XPS spectra of Fe2p in NiFe-LDH and NiFe-LDH/NEGF.

Table S3: Comparison of the XPS data of the present work with the different works published in the literature.

Sr. No.	Fe 2p (eV) (Fe2p _{1/2} , Fe2p _{3/2})	N1s (eV) (Pyriddic-N, Pyrrolic-N, Quaternary-N)	Ref.
1.	711.7, 725.0		5
2.		398.2, 399.2, 401.2	6
3.	711.9, 725.9		7
4.		397.45 (45.8 wt%), 399.06 (31.8 wt%), 400.41(22.4 wt%)	8
5.	710.9, 725.1	398.6 (42.4 wt%), 399.7 (41.6 wt%), 400.5 (15.9 wt%)	This Work

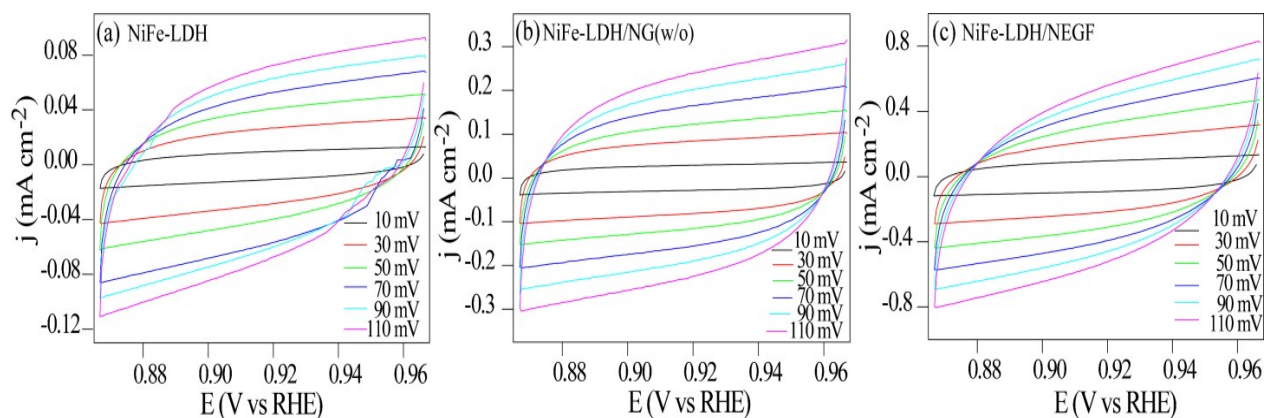


Figure S9: ECSA measurement through electrochemical double-layer charge capacitance (C_{dl}) measurement by recording CV in the non-Faradic region at different scan rates of 10 to 110 mV/s, (a) for NiFe-LDH, (b) for NiFe-LDH/NEGF(w/o), and (c) NiFe-LDH/NEGF.

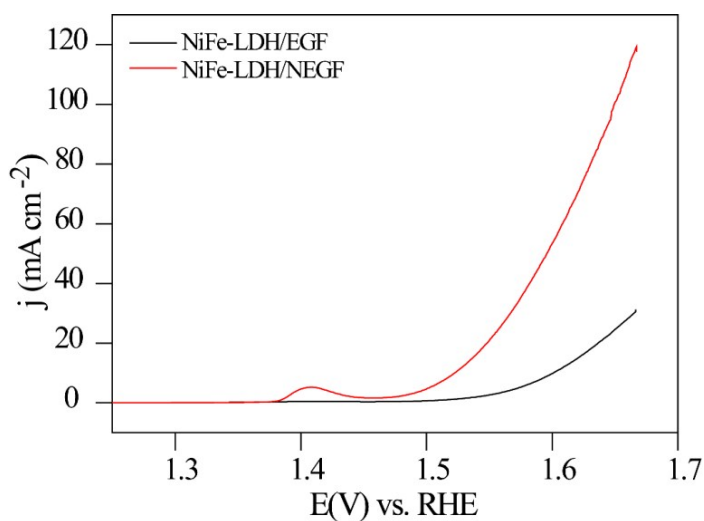


Figure S10: Comparative OER polarization curves of NiFe-LDH/NEGF and NiFe-LDH/EGF.

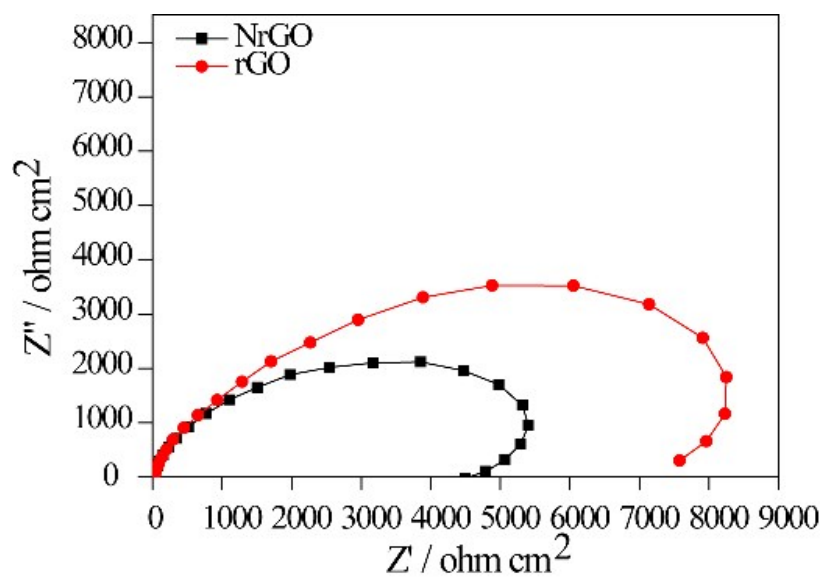


Figure S11: OER polarization curves recorded at 10 mV s^{-1} scan rate and 1600 rpm of the working electrode.

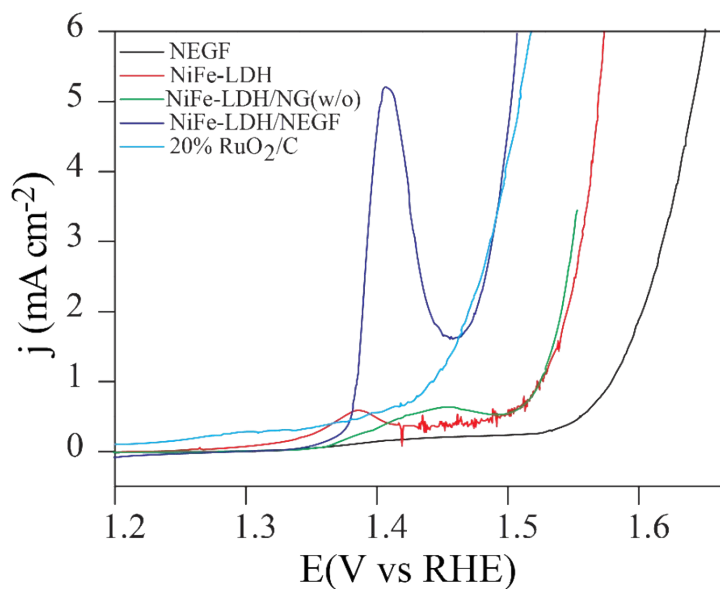


Figure S12: Nyquist plots recorded on rGO and NrGO at an applied potential of 1.57 V in the AC frequency range between 100 kHz and 0.1 Hz.

Table S4: OER activity data Comparison for the different synthesized catalysts.

Electrocatalysts	Overpotential (mV)	Double Layer Capacitance (C_{dl})	Tafel Slop ($mV\ dec^{-1}$)
NiFe-LDH	350 mV	1.1 $mF\ cm^{-2}$	72
NiFe-LDH/NG(w/o)	340 mV	3.9 $mF\ cm^{-2}$	71
NiFe-LDH/NEGF	290 mV	8.8 $mF\ cm^{-2}$	68
20% RuO_2/C	310 mV	-	108
NiFe-LDH/EGF	370 mV	-	-

Table S5: Comparison of the OER activity data of the present work with the different works published in the literature.

Sr. No.	Electrocatalyst	Overpotential (mV)	Electrolyte	Tafel slop ($mV/dec.$)	Ref.
1.	NiFe LDH/oGSH hybrid	350	0.1 M KOH	54	4
2.	NiFe LDH/C (Vulcan XC-72R)	360	0.1 M KOH	51	5
3.	NiFe LDH/CNT hybrid	308	0.1 M KOH	35	6
4.	NiFeOx fim	336	1.0 M KOH	30	7
5.	NiFe LDH	302	1.0 M KOH	40	8
6.	Ni-Fe	331	1.0 M KOH	58	9
7.	NiFe-LDH/NEGF	290	1.0 M KOH	68	This Work

References:

- [1]. D. C. Marcano, D. V. Kosynkin, J. M. Berlin, A. Sinitkii, Z. Sun, A. Slesarev, L. B. Alemany, W. Lu, and J. M. Tour, *Acs Nano*, 2010, **4**, 4806-4814.
- [2]. T. Audichon, T. W. Napporn, C. Canaff, C. Morais, C. Comminges, and K. B. Kokoh, *J. Phys. Chem. C*, 2016, **120**, 2562-2573.
- [3]. N. Ayasha, V. M. Dhavale and S. Kurungot, *Nanoscale*, 2017, **9**, 12590.

- [4]. V. A. Alves, L. A. da Silva, and J. F. C. Boodts, *Electrochimica Acta*, 1998, **44**, 1525-1534.
- [5]. R. Liang, L. Shen, F. Jing, N. Qin, and Li. Wu, *ACS Appl. Mater. Interfaces*, 2015, 7, 9507 –9515.
- [6]. S. Ci, S.u. Mao, Y. Hou, S. Cui, H. u. Kim, R. Ren, Z. e. Wen, and J. Chen, *J. Mater. Chem. A*, 2015, 3, 7986–7993.
- [7]. B. Weng, F. n. Xu, C. a. Wang , W.e. Meng, C. y. R. Grice, and Y. Yan, *Energy Environ. Sci.*, 2017, 10, 121-128.
- [8]. S. K. Singh, V. Kashyap, N. Manna , S. N. Bhange, R. Soni, R. Boukherroub, S. Szunerits, and S. Kurungot, *ACS Catal.* 2017, 7, 6700–6710.